Real-time wave excitation force estimation for an experimental multi-DOF WEC

A.J. Hillis[1], A. Brask[2], and C. Whitlam[2]

[1]University of Bath, Department of Mechanical Engineering, Bath BA27AY, UK. e-mail: a.j.hillis@bath.ac.uk

[2]Marine Power Systems Ltd, Ethos Building, Kings Road, Swansea, SA1 8AS. e-mail: contact@marinepowersystems.co.uk

Abstract

A wave energy converter (WEC) needs an active control strategy to maximise efficiency in a wide range of operating conditions. Many control strategies require knowledge of the wave excitation force, a quantity which cannot be measured in operation. In this study, two methods based upon Kalman filters are tested with an experimental 1:25th scale multiple degree-of-freedom WEC. A stochastic and a periodic Kalman estimator are implemented, using only quantities which are measurable in practice. Methods for tuning the estimators are discussed, and sensitivity to nonlinearity in the WEC and to unmodelled effects including quadratic viscous damping are established. The advantages of each method are compared, and excellent quality estimation results are obtained using both methods. Both methods are verified for use with advanced control strategies to improve power capture in WECs.

Keywords–Wave energy converter, wave excitation force, real-time estimation, experimental testing, Kalman filter.

I. Introduction

A wave energy converter (WEC) needs an active control strategy to maximise efficiency in a wide range of operating conditions. Most optimal and suboptimal WEC control strategies (e.g. Model Predictive Control (MPC) [1], [2], and Approximate Optimal Velocity Tracking (AVT) [3]) require knowledge of the wave excitation force acting on the prime mover. In practice this force cannot be measured, so it must be estimated. Several linear and nonlinear estimation options have been studied to achieve this in real-time, but most studies are simulation based and restricted to simplified linear systems. A review of many of these methods can be found in [4]. A popular approach is to use a Kalman Filter (KF) observer which assumes the excitation force can be represented as the sum of a finite set of harmonic components (e.g. [5], [6]). In [7] an extended KF approach is used which operates on pressure measurements on the WEC hull. Alternatively, in [8] a Fast Adaptive Unknown Input Estimation (FAUIE) observer is proposed and applied to a point-absorber WEC, and is further verified in [9]. In all cases, very good estimation performance is reported. Most of these studies focus on simplified 1-DOF systems in simulation, though in [10] a KF approach is extended and applied to arrays of 1-DOF WECs using both coupled and decentralised strategies. In [11], a periodic KF estimator is applied to a linearised 3-DOF simulation model of the ISWEC device. An example of an experimental study is described in [12], where two estimation methods are compared. One method uses a KF as an extended observer with a random-walk model to estimate a lumped unknown system disturbance. The second method uses a receding horizon MPC-like approach. Both methods are applied to a scale physical model of a Wavestar WEC float in a range of sea states and similarly accurate results are achieved using both methods.

In summary, many methods have been developed to estimate the excitation force in real time, but examples of experimental testing on multiple degree-of-freedom systems are sparse. In the present study, we apply two real-time methods for excitation force estimation to a scaled physical model of the WaveSub WEC - a nonlinear, multi-DOF submerged point absorber. The objective is to use a method that is simple, robust, and uses only readily measureable quantities to perform its estimation. To this end, the random-walk KF approach of [12] is compared against the periodic KF approach described in [11]. The design of the WEC, particularly the use of multiple taut tethers as the actuation input to the prime mover makes the estimation task particularly challenging. Further, the

comprehensive coverage of excitation regimes and consideration of the sensitivity of the estimation to KF tuning and unmodelled nonlinear effects distinguish this study from others.

The remainder of the paper is organised as follows. An overview of the WaveSub WEC is provided in section II. Section III provides a description of the forces acting on the WEC. A linearised system model for use by the excitation force estimators is provided in section IV. The estimation procedures are described in section V. The experimental setup is described in section VI and experimental results provided in section VII. The sensitivity of the estimators to the effects of viscous drag, Kalman filter tuning and system nonlinearity are discussed in sections VIII, IX and X, respectively. Finally, conclusions are provided in section XI.

II. The WaveSub WEC

WaveSub is under development by Marine Power Systems Ltd (MPS). It is a submerged point absorber with a unique multi-tether configuration and variable geometry which can be tuned to the prevailing sea state. This study focuses on a 1:25 scale experimental WEC which was tested throughout 2018 and 2019. The experimental WEC is shown in the photographs of Figure 1, located in the Ocean Basin wave tank at the University of Plymouth COAST laboratory. A float moves with the waves and reacts against a moored base. The float is attached to four taut tethers which pull on rotational drums which are attached to a power take-off (PTO). In the configuration pictured, the reactor measures 2m $\times$ 2m $\times$ 0.5m and is moored using four taut lines to the wave tank floor. Also shown in these pictures are Qualisys tracking system markers on the reactor and float, and a wave gauge in line with the float centre of gravity.

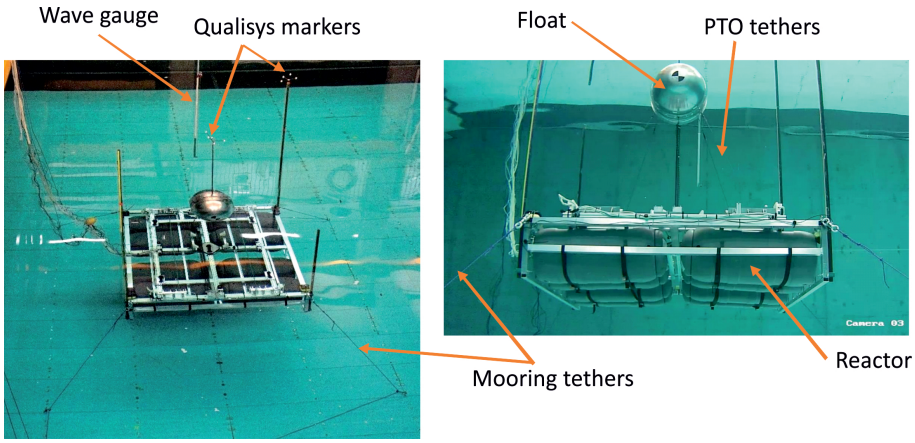

Fig. 1. Photgraphs of 1:25th scale experimental WEC. Left: from above surface Right: from below surface

Table I provides dimensions of the experimental WEC system.

TABLE I
DIMENSIONS OF THE GEOMETRY OF THE FULL SCALE WEC-SIM MODEL

Properties	Value	Unit
Float diameter	0.47	m
Float cylinder length	0.19	m
Float mass	68	kg
Reactor length	2.0	m
Reactor width	2.0	m
Reactor height	0.5	m
Water depth	3.0	m
Submergence (to top of float)	0.08	m
PTO spring stiffness	360	N/m

III. Forces acting on the WEC

Following the standard Cummins representation [13], the WEC equation of motion for the 6DOF state vector $\mathbf{x} = [x\ y\ z\ \theta_x\ \theta_y\ \theta_z]^T$ may be written as

$$(\mathbf{M} + \mathbf{A}_\infty)\,\ddot{\mathbf{x}}(t) + \int_0^t \mathbf{K}_r(t-\tau)\dot{\mathbf{x}}(\tau)d\tau + \mathbf{K}_0\mathbf{x}(t) = \mathbf{f}_e(t) + \mathbf{u}(t) \tag{1}$$

where $\mathbf{M}$ and $\mathbf{A}_\infty$ are the system mass and infinite added mass matrices, $\mathbf{K}_r$ is the radiation impulse response, and $\mathbf{K}_0$ is the system stiffness matrix resulting from passive springs acting on the PTO tethers. $\mathbf{f}_e$ and $\mathbf{u}$ are the 6DOF wave excitation and control force vectors imposed by the incident waves and the PTO, respectively. $\mathbf{A}_\infty$ and $\mathbf{K}_r$ are commonly estimated using a Boundary Element Method (BEM) solver, here we use NEMOH [14]. $\mathbf{M}$ and $\mathbf{K}_0$ are found from knowledge of the physical system properties. There is no hydrostatic stiffness term as the float is fully submerged, and the buoyancy force is balanced by the static spring force in the PTO tethers, therefore these forces are not included.

This formulation neglects viscous drag, which may be significant in some cases. For now we make the common assumption that viscous drag is small in comparison to the other forces, and a study of the effects of viscous drag is included in section VIII to justify this. The spring force and control force are imposed through the PTO system, which is discussed in section VI-B. The remaining hydrodynamic forces are discussed in the following sub-sections.

A. Idealised wave excitation force

The excitation force is not measurable, so must be estimated. This task is the central purpose of this investigation. Ideally, the excitation force would be experimentally determined by locking the float in position and measuring the loads on the float due to waves. This was not possible in this case as the investigation was conducted as part of a wider campaign to investigate the overall WEC concept feasibility. Even if it were possible, this procedure would not give an accurate measure of the excitation force under controlled conditions as the float location varies substantially within a wave. Therefore, the only means for comparison with experimentally estimated excitation forces comes from the linearised estimates resulting from BEM solutions, which have the same drawback in terms of float location, and additionally assume linear potential flow theory is valid. A numerical model of a 3-float embodiment of WaveSub has previously been developed using the WEC-Sim package [15]. The outputs of this 1:25 scale numerical model have been compared to wave tank experimental data at the same scale in [16]. The hydrodynamic co-efficients of a single float are used here to generate theoretical results as a means of comparison. Figure 2 shows an image of the float geometry and BEM mesh. The resulting excitation force frequency responses $H_e(\omega)$, obtained from the NEMOH BEM solver, are shown in Figure 3. For all the cases conducted in this study, the incident wave direction is axially aligned with the float, so motion mainly occurs in the surge (x), heave (z) and pitch (θ_y) DOFs. The geometry of the prime mover (float) is symmetric and identical in the surge and heave directions.

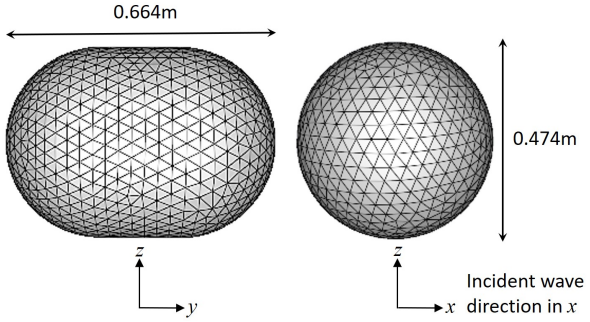

Fig. 2. Image of float geometry and BEM mesh

The non-causal BEM excitation impulse response function (IRF) of $H_e(\omega)$ is shown in Figure 4, and this can be used to generate a theoretical wave excitation force. Here we perform a post-process comparison, therefore we convolve the excitation IRF with a measured (and suitably time-shifted) wave elevation time history to generate a theoretical wave excitation force. The IRF can be causalised through a numerical fitting process, e.g. [9] if a real-time estimate is required.

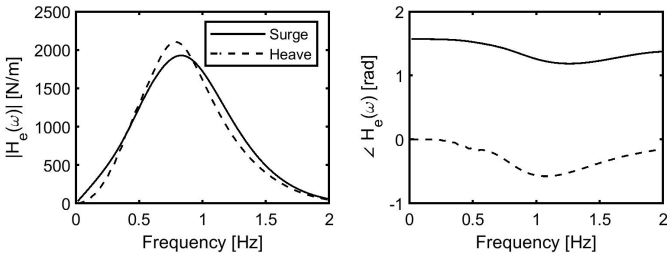

Fig. 3. Frequency response of float wave excitation force

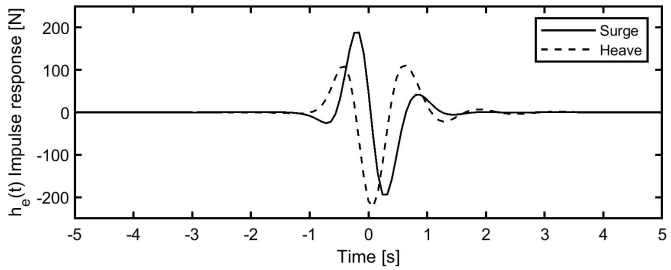

Fig. 4. Float wave excitation force impulse response functions in surge and heave

B. Radiation force

Figure 5 shows the radiation impulse response functions (from NEMOH) for the float. As is commonly done, these are approximated by 4^{th} order State-Space models of the form:

$$\begin{aligned} \dot{\mathbf{p}}_r(t) &= \mathbf{A}_r \mathbf{p}_r(t) + \mathbf{B}_r \dot{\mathbf{x}}(t) \\ \int_0^t \mathbf{K}_r(t-\tau)\dot{\mathbf{x}}(\tau)d\tau &\approx \mathbf{C}_r \mathbf{p}_r(t) + \mathbf{D}_r \dot{\mathbf{x}}(t) \end{aligned} \tag{2}$$

where the matrices $\{\mathbf{A}_r, \mathbf{B}_r, \mathbf{C}_r, \mathbf{D}_r\}$ describing $\mathbf{G}_r$ are computed using the BEMIO code, part of the WEC-Sim package. The impulse responses of the approximate models are also shown in Figure 5.

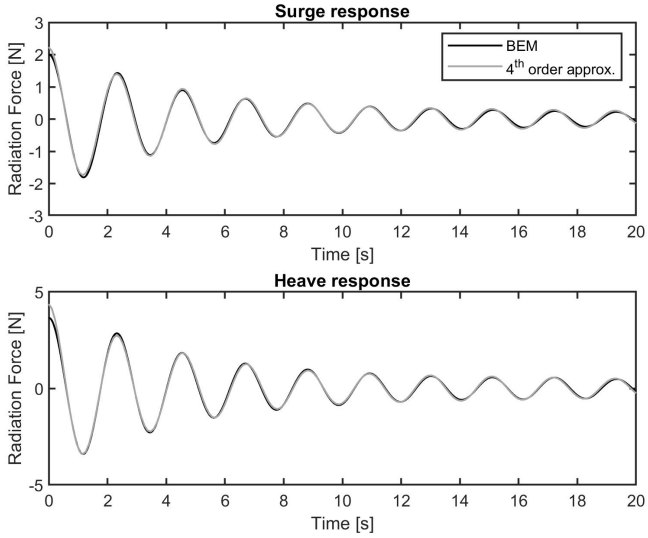

Fig. 5. Radiation force unit impulse responses for surge and heave

IV. Linearised dynamic system model

The Kalman filters used to estimate the excitation force require a linearised approximation to the WEC and PTO systems. For simplicity we assume the reactor to be fixed as a taut mooring system is used. Therefore, omitting the time dependence for clarity, the WEC dynamics can be represented by the state-space system

$$\begin{aligned} \begin{bmatrix} \dot{\mathbf{x}} \\ \ddot{\mathbf{x}} \\ \dot{\mathbf{p}}_r \end{bmatrix} &= \mathbf{A}_c \begin{bmatrix} \mathbf{x} \\ \dot{\mathbf{x}} \\ \mathbf{p}_r \end{bmatrix} + \mathbf{B}_c(\mathbf{f}_e + \mathbf{u} - \mathbf{K}_0\mathbf{x}) \\ \mathbf{y} &= \mathbf{C}_c \begin{bmatrix} \mathbf{x} \\ \dot{\mathbf{x}} \\ \mathbf{p}_r \end{bmatrix} \end{aligned} \tag{3}$$

where $\mathbf{x}$ is the state vector as defined in section III. For the float geometry studied here (please refer to Figure 2), there are nine significant radiation impulse response functions which need to be approximated (similar to the study in [17]). This results in 36 radiation force states $\mathbf{p}_r$ and the following system matrices:

$$\begin{aligned} \mathbf{A}_c \in \mathbb{R}^{48\times 48} &= \begin{bmatrix} \mathbf{0} & \mathbf{I} & \mathbf{0} \\ \mathbf{0} & -\mathbf{M}_\infty^{-1}\mathbf{D}_r & -\mathbf{M}_\infty^{-1}\mathbf{C}_r \\ \mathbf{0} & \mathbf{B}_r & \mathbf{A}_r \end{bmatrix} \\ \mathbf{B}_c \in \mathbb{R}^{48\times 6} = \begin{bmatrix} \mathbf{0} \\ \mathbf{M}_\infty^{-1} \\ \mathbf{0} \end{bmatrix} \quad \mathbf{C}_c &\in \mathbb{R}^{12\times 48} = \begin{bmatrix} \mathbf{I} & \mathbf{0} \end{bmatrix} \end{aligned} \tag{4}$$

where $\mathbf{M}_\infty$ is the sum of the float mass matrix and infinite added mass matrix obtained from the BEM solution. Note that the linearised stiffness matrix $\mathbf{K}_0$ is not included in the plant matrix $\mathbf{A}_c$ as the total PTO tether tension (including the control forces and contribution from springs) is directly measured. The state-space model is then discretized using a first-order hold approximation, such that

$$\begin{aligned} \begin{bmatrix} \mathbf{x} \\ \dot{\mathbf{x}} \\ \mathbf{p}_r \end{bmatrix}_{k+1} &= \mathbf{A} \begin{bmatrix} \mathbf{x} \\ \dot{\mathbf{x}} \\ \mathbf{p}_r \end{bmatrix}_k + \mathbf{B}(\mathbf{f}_{e,k} - \mathbf{T}_k) \\ \mathbf{y}_k &= \mathbf{C} \begin{bmatrix} \mathbf{x} \\ \dot{\mathbf{x}} \\ \mathbf{p}_r \end{bmatrix}_k \end{aligned} \tag{5}$$

$\mathbf{T}$ is the Cartesian vector of tether tension forces, derived from direct measurement of the combined control and spring forces $\mathbf{T}_{PTO}$ according to

$$\mathbf{T} = \mathbf{J}_0^{-T}\mathbf{T}_{PTO} \tag{6}$$

where $\mathbf{J}_0^{-T}$ is the transpose of the inverse kinematic Jacobian matrix [18] relating Cartesian and PTO tether spaces.

V. Wave Force Estimation

Assuming the linearised WEC model to be accurate, and assuming the availability of estimates or measurements of the float motion, it is possible to implement a dynamic observer to estimate the wave excitation force. Here we use two Kalman filter approaches - a stochastic method and a periodic method - to achieve this.

A. Stochastic method

This method is similar to the random-walk method described in [12]. The state vector is augmented with the unknown disturbance force $\mathbf{f}_e$. Adopting the notation $\mathbf{x}^+$ for the augmented state vector, the discretized system dynamics are now described by

$$\mathbf{x}^+_{k+1} = \begin{bmatrix} \mathbf{x} \\ \dot{\mathbf{x}} \\ \mathbf{p}_r \\ \mathbf{f}_e \end{bmatrix}_{k+1} = \mathbf{A}^+\mathbf{x}^+_k + \mathbf{B}^+ \left(\mathbf{f}_e - \mathbf{T}\right)_k + \boldsymbol{\epsilon}_k \tag{7}$$

$$\mathbf{y} = \mathbf{C}^+\mathbf{x}^+_k + \boldsymbol{\mu}_k$$

where $\boldsymbol{\epsilon}$ describes the random walk process for excitation force estimation and unmodelled dynamics, and $\boldsymbol{\mu}$ describes measurement noise. Including excitation force estimations for n DOFs, the system matrices are defined as follows:

$$\mathbf{A}^+ \in \mathbb{R}^{48+n\times 48+n} = \begin{bmatrix} \mathbf{A} & \mathbf{B} \\ \mathbf{0} & \mathbf{I} \end{bmatrix} \quad \mathbf{B}^+ \in \mathbb{R}^{48+n\times 6} = \begin{bmatrix} \mathbf{B} \\ \mathbf{0} \end{bmatrix} \quad \mathbf{C}^+ \in \mathbb{R}^{12\times 48+n} = \begin{bmatrix} \mathbf{C} & \mathbf{0} \end{bmatrix} \tag{8}$$

B. Periodic method

In this formulation, $\mathbf{f}_e$ is assumed to be the linear superposition of the outputs of a set of i harmonic oscillators at specified frequencies $[\omega_1 \dots \omega_i]$. We denote this form of excitation force as $\mathbf{F}_e$, and the augmented state vector is $[\mathbf{x}\ \dot{\mathbf{x}}\ \mathbf{p}_r\ \mathbf{F}_e\ \dot{\mathbf{F}}_e]^T$. The corresponding system matrices are given by

$$\mathbf{A}^+_c \in \mathbb{R}^{48+2ni\times 48+2ni} = \begin{bmatrix} \begin{bmatrix} \\ \mathbf{A}_c \\ \\ \end{bmatrix} & \begin{matrix} \mathbf{0} & \mathbf{0} \\ -\tilde{\mathbf{M}}_\infty^{-1} & \mathbf{0} \\ \mathbf{0} & \mathbf{0} \end{matrix} \\ \begin{matrix} \mathbf{0} \\ \mathbf{0} \end{matrix} & \begin{matrix} \mathbf{0} & \mathbf{I} \\ -\boldsymbol{\Omega}^2 & \mathbf{0} \end{matrix} \end{bmatrix}$$
$$\mathbf{B}^+_c \in \mathbb{R}^{48+2ni\times 6} = \begin{bmatrix} [\mathbf{B}_c] \\ \mathbf{0} \\ \mathbf{0} \end{bmatrix} \quad \mathbf{C}^+_c \in \mathbb{R}^{12\times 48+2ni} = \begin{bmatrix} \mathbf{C}_c & \mathbf{0} & \mathbf{0} \end{bmatrix} \tag{9}$$

where $\boldsymbol{\Omega}$ is the diagonal matrix of specified excitation frequencies for each of n DOFs, i.e. for all 6DOFs,

$$\boldsymbol{\Omega} \in \mathbb{R}^{ni\times ni} = \begin{bmatrix} \Omega_x & 0 & 0 & 0 & 0 & 0 \\ 0 & \Omega_y & 0 & 0 & 0 & 0 \\ 0 & 0 & \Omega_z & 0 & 0 & 0 \\ 0 & 0 & 0 & \Omega_{\theta_x} & 0 & 0 \\ 0 & 0 & 0 & 0 & \Omega_{\theta_y} & 0 \\ 0 & 0 & 0 & 0 & 0 & \Omega_{\theta_z} \end{bmatrix} \tag{10}$$

where, e.g. for the x-direction,

$$\Omega_x \in \mathbb{R}^{i\times i} = \begin{bmatrix} \omega_1 & 0 & 0 & 0 \\ 0 & \omega_2 & 0 & 0 \\ 0 & 0 & \ddots & 0 \\ 0 & 0 & 0 & \omega_i \end{bmatrix} \tag{11}$$

$\tilde{\mathbf{M}}_\infty$ is a manipulation of the mass matrix $\mathbf{M}_\infty$ to correctly map the excitation force vectors to accelerations, i.e.

$$\tilde{\mathbf{M}}_\infty = \mathbf{M}_\infty\tilde{\mathbf{I}} \tag{12}$$

where $\tilde{\mathbf{I}}$ is an n-block diagonal matrix of the vectors $[1, ..., 1] \in \mathbb{R}^{1\times i}$. The discretized system dynamics are now described by

$$\mathbf{x}_{k+1}^{+} = \begin{bmatrix} \mathbf{x}^{+} \\ \mathbf{F}_e \end{bmatrix}_{k+1} = \mathbf{A}^{+}\mathbf{x}_k^{+} - \mathbf{B}^{+}\mathbf{T}_k + \boldsymbol{\epsilon}_k$$
$$\mathbf{y} = \mathbf{C}^{+}\mathbf{x}_k^{+} + \boldsymbol{\mu}_k \tag{13}$$

which is similar to equation 7 for the stochastic estimator, and the definition of variance terms is identical.

C. Kalman Filter implementation

Once the discretized system matrices are obtained as detailed in sections V-A and V-B, the wave excitation force can be estimated by implementing a standard Kalman filter. The prediction step estimates the next state $\hat{\mathbf{x}}_{k|k-1}^{+}$ and covariance $\mathbf{P}_{k|k-1}^{+}$ matrices as:

$$\begin{aligned} \hat{\mathbf{x}}_{k|k-1}^{+} &= \mathbf{A}_{k-1}^{+}\hat{\mathbf{x}}_{k-1|k-1}^{+} + \mathbf{B}^{+}\mathbf{T}_{k-1|k-1} \\ \mathbf{P}_{k|k-1}^{+} &= \mathbf{J}_{k-1}^{+}\mathbf{P}_{k-1|k-1}^{+}\mathbf{J}_{k-1}^{+T} + \mathbf{Q}_{k-1}^{+} \end{aligned} \tag{14}$$

where $\mathbf{Q}^{+}$ is the process noise covariance matrix which provides weighting values for the states associated with the WEC DOFs $\mathbf{Q}_n$ and the excitation force estimates $\mathbf{Q}_{\hat{F}_e}$, i.e.

$$\mathbf{Q}^{+} = \begin{bmatrix} \mathbf{Q}_n & \mathbf{0} \\ \mathbf{0} & \mathbf{Q}_{\hat{F}_e} \end{bmatrix} \tag{15}$$

The update step is defined by:

$$\begin{aligned} \mathbf{S}_k^{+} &= \mathbf{C}_k^{+}\mathbf{P}_k^{+}\mathbf{C}_k^{+T} + \mathbf{R}_k^{+} \\ \mathbf{K}_k^{+} &= \mathbf{P}_k^{+}\mathbf{C}_k^{+T}\mathbf{S}_k^{+^{-1}} \\ \hat{\mathbf{x}}_{k|k}^{+} &= \hat{\mathbf{x}}_{k|k-1}^{+} + \mathbf{K}_k^{+}\left(\begin{bmatrix}\mathbf{y}_k & \hat{\mathbf{F}}_e\end{bmatrix}^{T} - \mathbf{C}_k^{+}\hat{\mathbf{x}}_{k|k-1}^{+}\right) \\ \mathbf{P}_{k|k}^{+} &= (I - \mathbf{K}_k^{+}\mathbf{C}_k^{+})\mathbf{P}_{k|k-1}^{+} \end{aligned} \tag{16}$$

where $\mathbf{S}^{+}$ is the innovation residual, $\mathbf{R}^{+}$ is the observation covariance associated with the observed value $\mathbf{y}$, and $\mathbf{K}^{+}$ is the Kalman gain. $\mathbf{J}^{+}$ is the Jacobian of $\mathbf{A}^{+}$. For a time invariant state transition matrix (as assumed here) this is equal to $\mathbf{A}^{+}$. For the stochastic method, the estimation of the wave excitation force $\hat{\mathbf{f}}_e$ is directly obtained while, for the periodic estimator, it is obtained from

$$\hat{\mathbf{f}}_e = \tilde{\mathbf{I}}\hat{\mathbf{F}}_e^{T} \tag{17}$$

Notes on tuning of the covariance matrices are included in section IX.

VI. Experimental setup

Experiments were conducted at the Plymouth COAST laboratory throughout 2018/2019 with a broad objective of testing and verifying various conceptual ideas for the WaveSub WEC.

A. Wave Tank Layout

Figure 6 shows a basic layout of the Ocean Basin wave tank at the COAST lab. The tank is 35m long and 15.5m wide, with wave makers at one end and a parabolic beach at the other. Regular and irregular sea states can be generated. The wave field was measured with several wave gauges, but only the wave gauge in line with the WEC float is indicated, as this is the relevant measurement point for the present study. This was located 2.5m from the float to avoid reflections from the WEC. The tank was allowed to settle between tests to further avoid the effects of reflections. Power and sensor signals are passed via umbilical lines to the gantry, where instrumentation and data logging hardware was located. A water depth of 3m was used for all test results presented here.

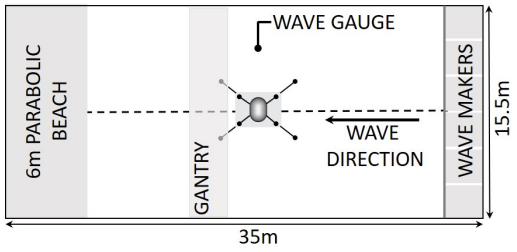

Fig. 6. Diagram of wave tank experimental layout

B. Experimental WEC

With reference back to Figure 2, the float is connected to the reactor by four taut tethers. These tethers are wrapped around drums and attached to the reactor by passive springs. The drums are connected to Maxon EC90 48V brushless DC motors, which are controlled by four-quadrant Maxon controllers to provide control torques. The motors are also connected to continuously variable rheostats enabling purely dissipative control. The drum rotational positions are measured using IP68 sealed RLS magnetic encoders. PTO and mooring tether loads are measured using Richmond Industries 200 series in-line 2kN load cells. These components are shown in the photographs of Figure 7.

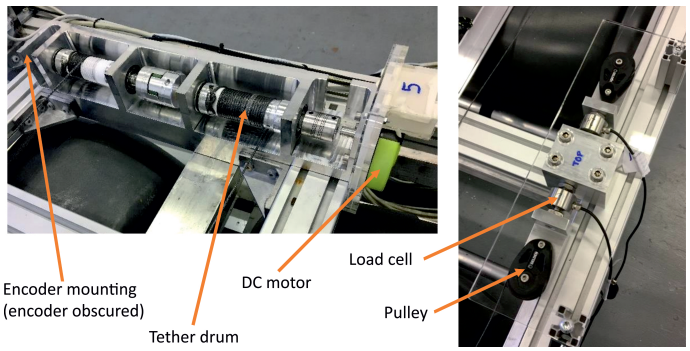

Fig. 7. Photographs showing PTO and measurement components

Signals were processed and logged via two NI PCI-6225 Multifunction DAQ units. The control loop was executed at 2kHz and data was logged at 100Hz. A trigger signal from the wavemakers was also logged to enable temporal alignment of data sets with wave data. Figure 8 shows a block diagram of the instrumentation setup. This equipment was originally constructed for a 3-float variant of the WaveSub WEC with 15 PTOs, hence the over-specified number of channels. Here only a reduced number of the available channels were utilized. In addition to the embedded instrumentation, the position of the float and reactor was tracked using a Qualisys system. This allows verification of float position estimation using PTO encoders.

VII. Experimental Results

Both regular and irregular wave cases were conducted with passive PTO damping provided through rheostats. For regular cases, the rheostat settings were swept through a set of discrete values during a test in order to change the PTO damping forces and obtain the optimum setting for power capture for a given wave period. For irregular cases, these optimal settings were used according to the dominant wave period and maintained throughout a test. Figure 9 shows the normalised captured power in regular waves of a range of periods and the same wave amplitude using the optimal rheostat settings. The passive springs attached to PTO drums were designed to achieve a natural frequency of approximately 0.5Hz, which is confirmed by the peak captured power.

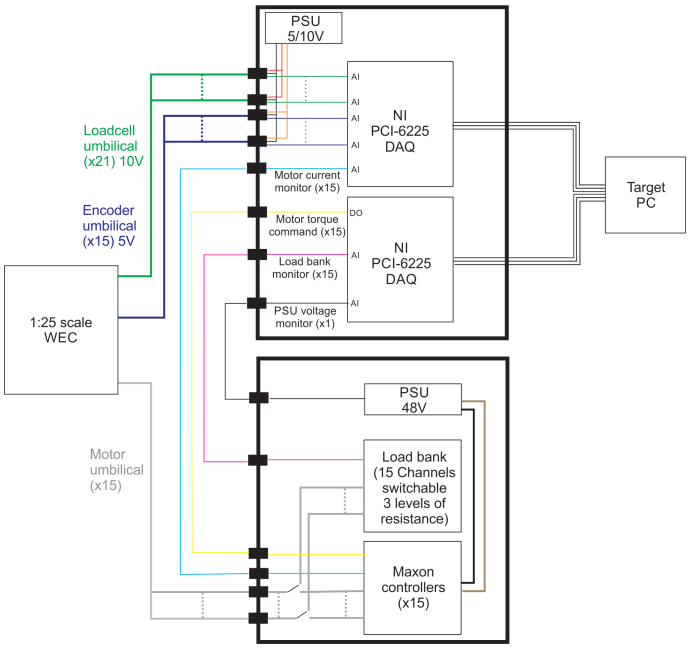

Fig. 8. Block diagram illustration of experimental instrumentation

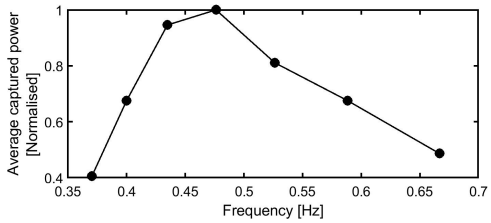

Fig. 9. Average captured power in regular waves of different periods.

A. Regular Waves

Results are presented here for three experimental regular wave cases. The amplitude spectra and wave elevation traces are shown in Figure 10

The wave excitation force spectra were pre-computed using the BEM-derived excitation impulse responses and numerically generated regular waves of the same amplitude and frequency as the experimental cases. This is necessary for estimating the frequencies required by the periodic estimator, but is not required for the stochastic estimator. The theoretical excitation force amplitude spectra for the three experimental regular cases are shown in Figure 11.

For compactness of presentation, detailed results are presented only for one regular wave case. The normalised excitation force power spectra for case R3 are shown in Figure 12. The dots mark the frequencies and state estimation weights specified in the surge and heave directions for use in the periodic estimator.

Both excitation force estimators require inputs of the measured float motion and PTO tether forces in Cartesian space. The float position is directly measured in Cartesian space during the experimental testing using a Qualisys system. The velocity is then calculated as the time derivative of float position. However, this information is not available in real-time to the instrumentation system. Instead, the PTO tether extension is directly measured using encoders and the velocity again obtained as the time derivative of extension. The PTO tether velocity is then transposed to Cartesian space using the inverse Jacobian in the same manner as for PTO tether forces in equation 6.

Figure 13 shows the velocities derived from both Qualisys and encoder measurements. It is clear that the quality of velocity estimation using the encoders is very good. There is an apparent under-

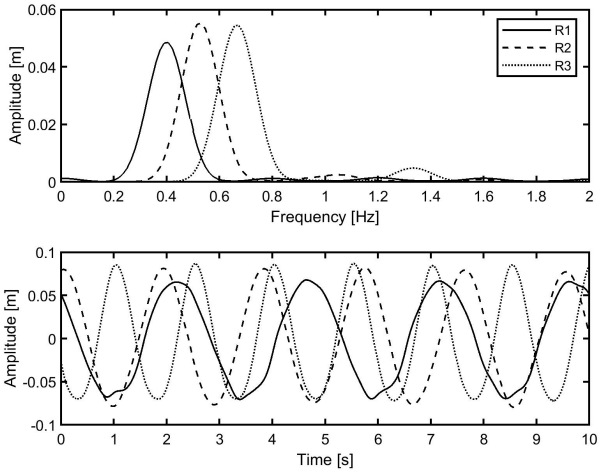

Fig. 10. Wave elevation and amplitude spectra for regular wave cases

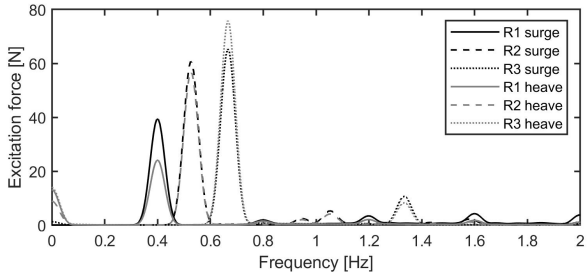

Fig. 11. Excitation force amplitude spectra for regular wave cases

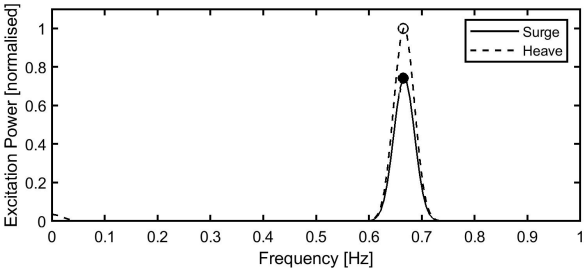

Fig. 12. Normalised excitation force power spectra for case R3

estimate of the surge velocity by approximately 10%, however this actually not the case. This effect is due to additional dynamics associated with the flexible pole attached to the top of the float holding the Qualisys markers. The effect is more apparent for irregular cases shown in section VII-B. For a full-scale deployment it may be desirable to directly measure the float motion, rather than infer it from encoder measurements. This could be achieved using an inertial measurement unit (IMU) located inside or on the surface of the float.

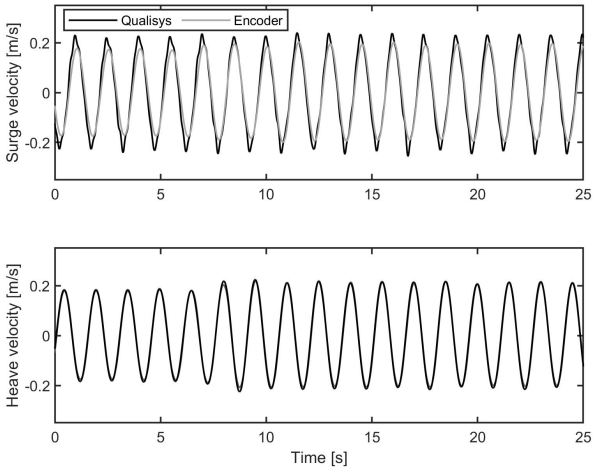

Fig. 13. Comparison of float velocities derived from Qualisys and encoder measurements for case R3

Figure 14 shows the directly measured PTO tether forces and the corresponding forces transformed to the surge and heave directions. At approximately 7s a step is seen where the the rheostats were adjusted in order to change the PTO damping. The Cartesian forces are provided as inputs to the excitation force estimators. It should be noted that each test had a duration of several hundred seconds, but only short sections of data are presented for clarity.

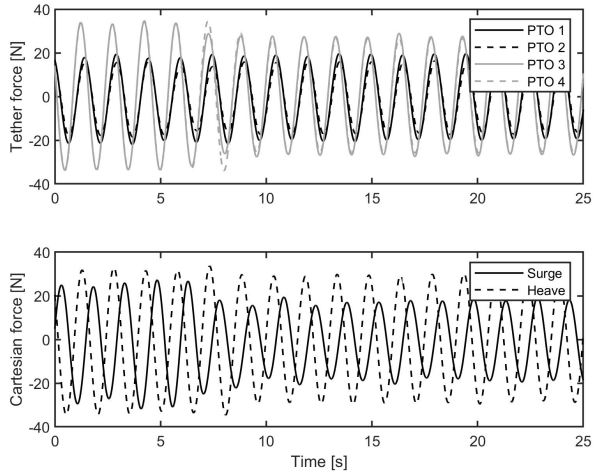

Fig. 14. PTO tether and Cartesian forces for case R3

Figure 15 shows the estimated wave excitation forces in the surge and heave directions, plotted against the theoretically derived values. Clearly there is excellent agreement and, as previously stated, there are going to be inaccuracies associated with both the theoretical results and the experimentally estimated values. What is also clearly shown is that both the stochastic and periodic estimators give very good results. This procedure was applied to all three regular sea states, and the goodness-of-fit values are provided in table II, evaluated over the full test duration. The normalised mean squared error goodness-of-fit measure used here is defined as

$$\mathrm{GOF} = 1 - \frac{\|\mathbf{f}_\mathrm{e} - \hat{\mathbf{f}}_\mathrm{e}\|^2}{\|\mathbf{f}_\mathrm{e} - \bar{\mathbf{f}}_\mathrm{e}\|^2} \tag{18}$$

where $\bar{\mathbf{f}}_e$ is the mean value of the vector $\mathbf{f}_e$ and $\|$ denotes the Euclidean norm of a vector.

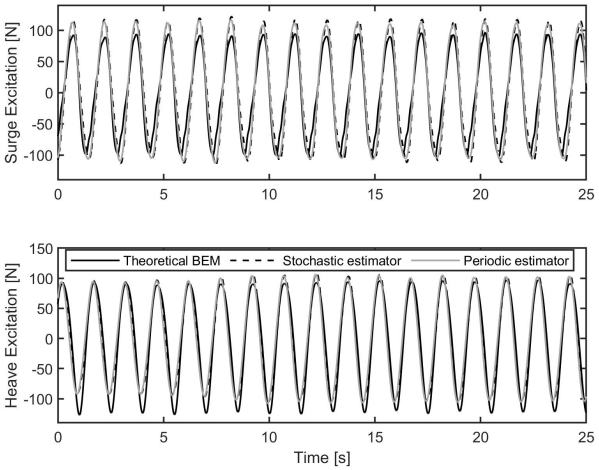

Fig. 15. Theoretical and experimentally estimated wave excitation forces for case R3 using stochastic and periodic estimators

TABLE II
WAVE PROPERTIES AND EXCITATION FORCE ESTIMATES GOF FOR REGULAR AND IRREGULAR CASES

Sea State			Excitation force estimation GOF [normalised]			
			Stochastic		Periodic	
Regular	Period [s]	Wave height [m]	Surge	Heave	Surge	Heave
R1	2.50	0.16	0.73	0.75	0.73	0.78
R2	1.90	0.16	0.95	0.89	0.95	0.92
R3	1.50	0.16	0.86	0.96	0.90	0.91
Irregular	Energy Period [s]	Sig. wave height [m]	Surge	Heave	Surge	Heave
I1	2.46	0.12	0.79	0.82	0.84	0.83
I2	2.22	0.12	0.81	0.87	0.86	0.87
I3	1.97	0.12	0.83	0.89	0.88	0.86
I4	1.75	0.12	0.84	0.84	0.89	0.77
I5	1.75	0.08	0.83	0.72	0.87	0.64
I6	1.75	0.16	0.87	0.85	0.92	0.78
I7	1.75	0.20	0.85	0.89	0.90	0.83

B. Irregular Waves

Results are presented here for four experimental irregular wave cases. The amplitude spectra and wave elevation traces are shown in Figure 16.

As for the regular wave cases, the irregular wave excitation force spectra were pre-computed using the BEM derived frequency responses and numerically generated irregular waves of the same peak amplitude and frequency as the experimental cases. This is necessary for estimating the frequencies required by the periodic estimator, but is not required for the stochastic estimator. The theoretical excitation force amplitude spectra for the four experimental irregular cases are shown in Figure 17. A small DC bias can be seen in the Heave excitation, which is a result of minor offset in the experimental data.

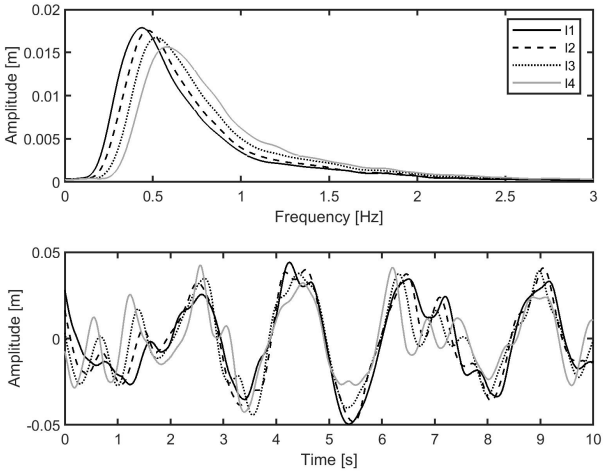

Fig. 16. Wave elevation and amplitude spectra for irregular wave cases

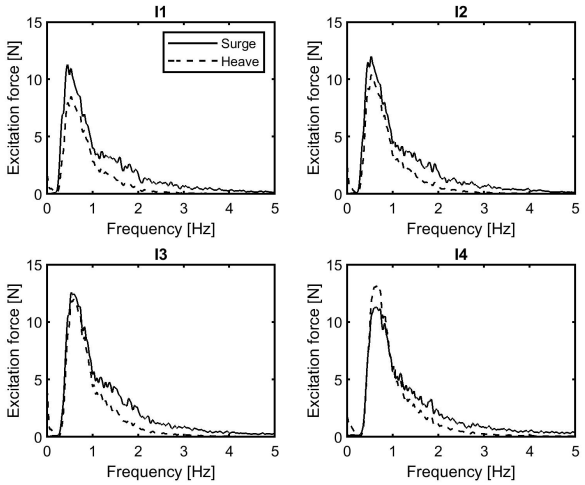

Fig. 17. Excitation force amplitude spectra for irregular wave cases

Again, for compactness of presentation, detailed results are presented only for one irregular wave case. The normalised excitation force power for case I3 is shown in Figure 18. The dots mark the specified frequencies and corresponding Kalman state estimation weights for the periodic estimator. In these cases 12 evenly spaced frequencies were selected to cover the majority of the excitation spectra. Sensitivity to this selection is discussed in section IX.

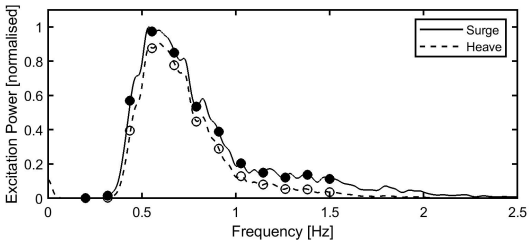

Fig. 18. normalised excitation force power for case I3

Figure 19 shows the velocities derived from both Qualisys and encoder measurements. As for the regular cases, excellent correlation is seen. A high frequency ripple is noticeable on the Qualisys data, particularly in the surge direction. This is due to a resonance of the Qualisys marker pole mounted on top of the float, and is not a physical property of the WEC.

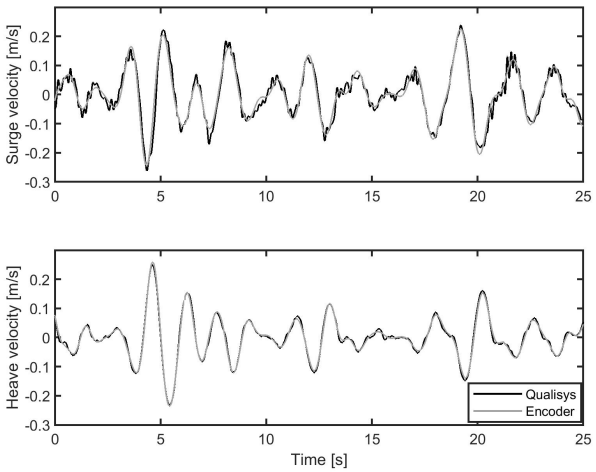

Fig. 19. Comparison of float velocities derived from Qualisys and encoder measurements for case I3

Figure 20 shows the directly measured PTO tether forces and the corresponding forces transformed to the surge and heave directions.

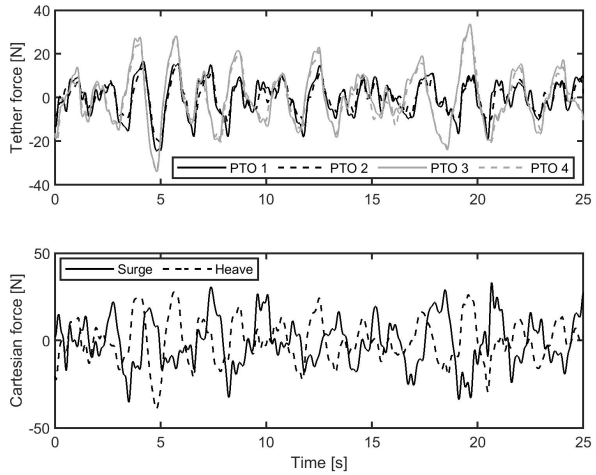

Fig. 20. PTO tether and Cartesian forces for case I3

Figure 21 shows the estimated wave excitation forces in the surge and heave directions, plotted against the theoretically derived values. There is excellent agreement and, again, both the stochastic and periodic estimators give very similar results. This procedure was applied to all four irregular sea states, and the goodness-of-fit values are provided in table II. The full test duration in each case was 700s.

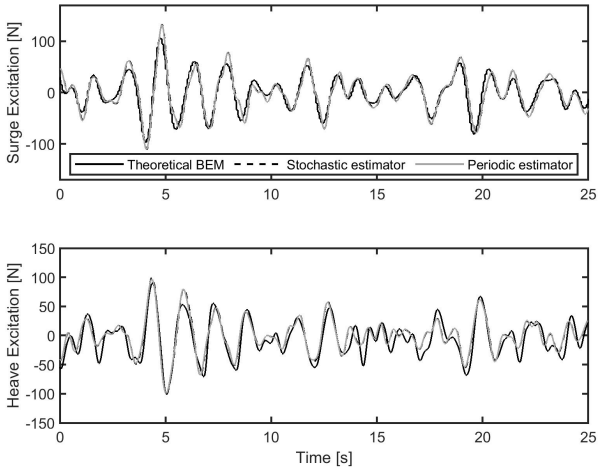

Fig. 21. Theoretical and experimentally estimated wave excitation forces for case I3 using stochastic and periodic estimators

VIII. A NOTE ON VISCOUS DRAG FORCES

At the outset of this study, it was assumed that viscous drag forces acting on the float were negligible. This is in line with many other studies, and is experimentally demonstrated in, for example [19] for a scaled physical model of a Wavestar WEC arm. The nature of the WEC in the present study is very different, and there is little in the literature for such a device with regard to viscous drag forces. Farraggiana includes a quadratic damping term based on the float velocity for the WaveSub WEC in a multi-float configuration [16]. However, this is an approximation as the drag force is actually dependent on the relative velocity between the float and the wave particle velocity. Here we calculate the wave particle velocity using Airy wave theory in order to estimate the relative velocity. We then calculate the quadratic drag force according to (for surge and heave directions only)

$$\begin{bmatrix} F_{v,x} \\ F_{v,z} \end{bmatrix} = -0.5\rho C_d A \begin{bmatrix} v_x^* & 0 \\ 0 & v_z^* \end{bmatrix} \begin{bmatrix} |v_x^*| \\ |v_z^*| \end{bmatrix} \tag{19}$$

where $v_{x,z}^*$ is the relative velocity in the x or z direction (surge or heave). Due to the symmetry of the float, the characteristic area A and drag coefficient C_d are the same for both directions. The velocities are plotted in Figure 22 for irregular wave case I3 with no viscous drag applied. This particular case is appropriate as the natural frequency of the WEC is tuned be approximately 0.5Hz, therefore it is near resonance.

The drag coefficient would be expected to be in the range 0 to 1, but it is difficult to estimate the appropriate drag coefficient to apply. Here we are not concerned with obtaining an exact match, only in studying whether the drag forces are significant or not. Therefore the drag forces were computed for a range of values of C_d, and these are plotted for wave case I3 in Figure 23. The peak values for the highest drag coefficient are less than 4% of the peak values of excitation force, which is in line with the findings in other studies (e.g. [19]). Therefore we can conclude that the viscous drag forces are negligible here. For a well-controlled WEC we would expect a significant increase in the float velocity, which could result in increased drag forces, however they will still be an order of magnitude below the wave excitation forces and PTO forces. If they were significant for a particular application, then the quadratic viscous drag forces may be readily calculated in real time and lumped with $\mathbf{F}_{PTO}$ as an external input force to the estimators. Alternatively, they may be linearised according to [20] and embedded within the estimators.

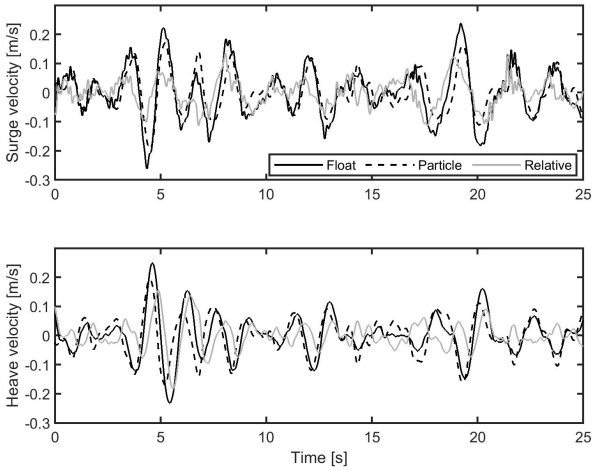

Fig. 22. Wave particle, float and relative velocities in irregular wave case I3

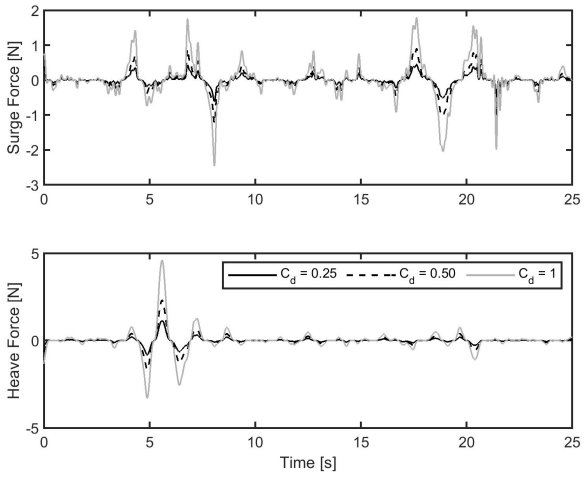

Fig. 23. Quadratic drag forces for different drag coefficients in irregular wave case I3

IX. A NOTE ON KALMAN FILTER TUNING

In the KF estimation procedures, the relative values of the **Q** and **R** matrices determine the estimation performance. These are tuned based upon knowledge of the covariance of the states (process) and outputs (measurements). Tuning in practice is often not intuitive, and it is often difficult to estimate the covariance of the process noise. As a result, it is common practice to empirically tune the KF *in-situ* . It is therefore important to understand the sensitivity of the estimation performance to this tuning. It should be noted that, to an extent, the success of the tuning process here is determined by comparison with a "known" excitation force. In reality the excitation is unknown so this presents a problem. Here we could argue that the relevant tuning parameters be increased until the output estimate does not change significantly, as shown in the following subsections. More rigorous possibilities also exist, for example in [21] a Gaussian process latent force model is presented as an alternative to the KF. In this work a maximum likelihood optimisation is employed to tune parameters rather than relying on an empirical approach.

A. Stochastic KF

The measurement noise covariance is easy to estimate, and $\mathbf{R}$ is used to normalise $\mathbf{Q}$, such that $\mathbf{R} = \mathbf{I}^{n\times n}$. The state covariances associated with the float DOFs ($\mathbf{Q}_n$) are empirically tuned to 100 times $\mathbf{R}$. Figure 24 shows the estimation performance (in terms of GOF compared to the theoretical excitation force estimation for case I3) as the terms in $\mathbf{Q}_{\hat{F}_e}$ relating to the excitation force estimation are varied. As the estimation problems for surge and heave are very similar, the same weight is used for both directions. It is seen that the GOF does not improve significantly for values beyond 2×10^9 for $\mathbf{Q}_{\hat{F}_e}$, therefore this value was selected and used to generate prior results.

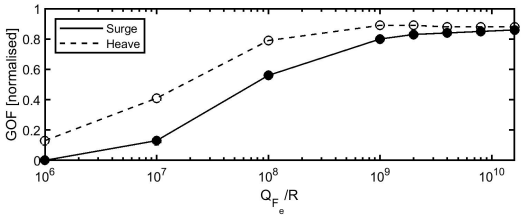

Fig. 24. Goodness-of-fit values for excitation force estimation using different estimation weights with stochastic KF estimator for case I3

B. Periodic KF

For the periodic estimator, the tuning of $\mathbf{Q}_n$ and $\mathbf{R}$ are exactly as for the stochastic estimator. What remains is to study the sensitivity of the excitation force estimation to the choice of $\mathbf{Q}_{\hat{F}_e}$ in terms of the number and distribution of frequencies included, and the associated weights. As previously stated, we followed the example of [11] with 12 evenly spaced frequencies, using the power spectrum of the excitation force as the weighting function. Figure 25 shows some of the tested distributions of oscillators. A single frequency centred on the power spectrum peak was used, then two frequencies either side of the peak. From then on the frequencies are evenly distributed across the peak and the number increased between 4 and 32. Again, results are presented for case I3.

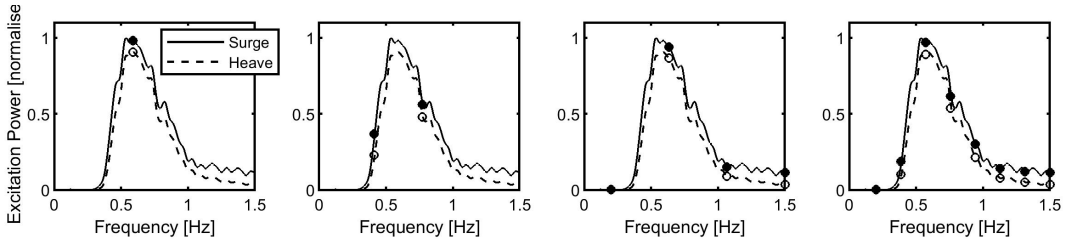

Fig. 25. Excitation force power spectra showing weights for different choices of oscillator numbers for period Kalman estimator. From left to right: $i = 1, 2, 4, 8$ for case I3

Figure 26 shows the GOF of the periodic estimator for the range of tested oscillator distributions.

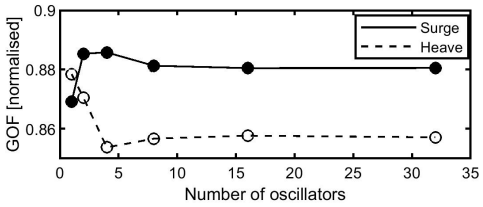

Fig. 26. Goodness-of-fit values for excitation force estimation using different numbers of oscillators with periodic KF estimator for case I3

It is seen that the estimation performance is largely insensitive to the number of frequencies, providing they are chosen to be on the peak of the excitation spectrum. Indeed, excellent performance

was achieved with a single frequency, though this performance would degrade sharply the further from the (*a priori* unknown) peak frequency it is located.

It is also important to investigate the sensitivity to the value of the weights. Insensitivity was established by selecting a flat unity weight for all 12 values of $\mathbf{Q}_{\hat{F}_e}$. Similarly good performance was achieved compared to the use of spectrally defined weights, with GOF values $\{0.87, 0.87\}$ as compared to $\{0.88, 0.86\}$ for spectrally defined weights.

Overall, both estimators perform very similarly. The stochastic estimator is computationally lighter, particularly if a large number of oscillators must be used with the periodic estimator. Figure 27 shows the computation time of one iteration (averaged over 1×10^5 iterations) of the periodic estimator in isolation for different numbers of oscillators. The computational time is normalised against the average time for a single iteration of the stochastic estimator using the same computer (again averaged over 1×10^5 iterations).

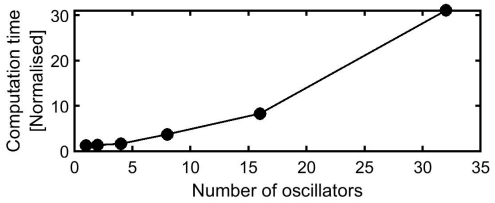

Fig. 27. Computation time for one iteration of stochasitc estimator compared to periodic estimator

Additionally, the periodic estimator requires prior knowledge of the excitation force spectra for each DOF if we are to guarantee good performance in a given sea state. This information may not be trivial to obtain *a priori* . The disadvantage of the stochastic estimator is that it will lump all unmodelled disturbances together in one estimate. This will mean that the excitation force estimate will be corrupted by model mismatch between the real WEC and the simplified model embedded in the estimator. In this respect, the periodic estimator will be more robust with large model mismatch, except if the model mismatch is in the estimation frequency range, in which case it will be indistinguishable from excitation disturbances.

X. A NOTE ON AMPLITUDE DEPENDENT NONLINEARITY

It is important to consider the effects of system nonlinearity. The WEC is inherently a nonlinear system, primarily because the stiffness matrix is dependent upon the position of the float. The method for estimating the excitation force, however, uses a linearised model of the WEC. Therefore there will be model mismatch which could affect the accuracy of estimation. In order to establish if this effect is significant here, we use the data from a set of irregular wave sets with the same energy period (1.75s) and initial phase, but with significant wave heights ranging from 0.08m to 0.2m. The position of the float for the different cases is plotted in Figure 28. At 1:25th scale the motion in the highest amplitude sea state represents an extreme operating case.

The GOF of the estimated wave excitation force for both stochastic and periodic estimators, compared to the theoretical values, is plotted against the different wave heights in Figure 29. It is seen that there is little effect on GOF as the wave height is increased, therefore we can conclude that the estimation procedure is robust to nonlinear model mismatch for this WEC.

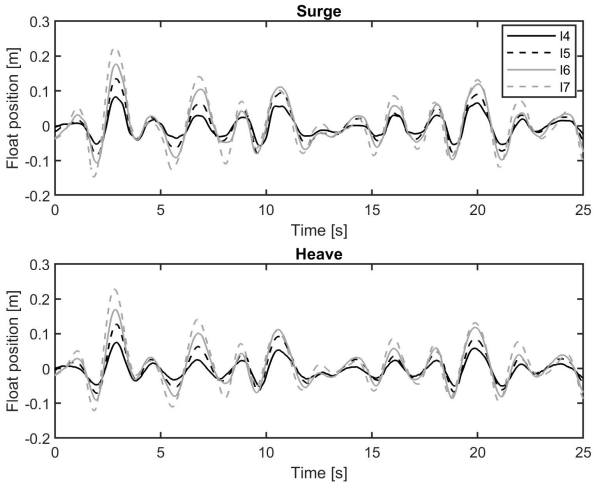

Fig. 28. Float position for irregular wave cases I4 to I7

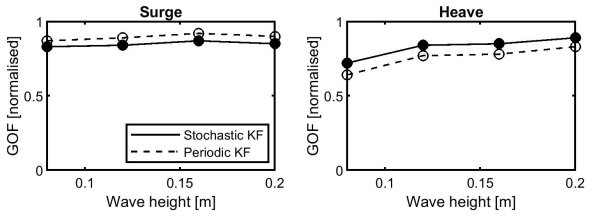

Fig. 29. Goodness-of-fit of wave excitation force compared to theoretical values for irregular wave cases I4 to I7

XI. Conclusions

Two methods for wave excitation force estimation have been investigated using an experimental 1:25th scale multi-DOF submerged point absorber WEC. Both methods utilise a Kalman filter to form an extended observer, simultaneously estimating system states and unknown disturbance forces as augmented states. One formulation uses a stochastic method based upon a random walk model, while the other method assumes the excitation force to be the super-position of multiple oscillator outputs at pre-defined frequencies.

Both methods were tested experimentally, using only quantities which are practically measurable in a real WEC, and excellent estimation performance was found in both cases. Further tests were conducted to establish the sensitivity of the Kalman filter estimators to un-modelled quadratic viscous drag forces, amplitude-dependent nonlinearity in the WEC and Kalman filter tuning. Both methods were found to be robust in all situations, providing the tuning is adequate.

The advantages of the stochastic estimator are computational ease and the lack of required *a priori* knowledge of the excitation spectra for the current sea state. The periodic estimator requires this *a priori* information in order to ensure the selection of oscillator frequencies adequately captures the excitation spectra, and it may not be trivial to obtain this information and adjust the estimator *in-situ*. On the other hand, selection of the number of oscillators (above a certain point) and weighting of each oscillator were not found to be critical to good performance, so it is conceivable that a static estimator could be constructed to adequately cover a wide range of operating conditions, all be it with a relatively high computational burden. The advantage of the periodic estimator is that the estimated excitation force is inherently bandwidth-limited by the selection of oscillator frequencies. The stochastic estimator will lump all unmodelled disturbances, meaning that the excitation force estimation will be corrupted by any unmodelled system dynamics.

The caveats associated with this study are as follows. For the experimental tests conducted, a purely dissipative control was used. While the system is tuned for resonance using passive springs, the motions of the float still may not be as large as they could be under active control. A study

was included of amplitude-dependent nonlinearity which included cases with large motions, and in practice an active control strategy would seek to constrain motion above this level. Therefore, we consider the cases presented here to be representative of real operating conditions. For the lack of any other practical comparison, estimated excitation forces are compared to theoretical values. These theoretical values are calculated using BEM-derived information about the float which is not necessarily accurate for complex geometries. However, due to the simplicity and symmetry of the float geometry here this is not a concern. We acknowledge that the means of comparison does not constitute a full validation of the methods, but we would also argue that a full validation is not possible, even with experimentally measured excitation forces achieved by locking the float in position. Indeed this issue is the very essence of the requirement for estimation - there is no means of measuring the true excitation force in practice. The resulting correlation is nonetheless very good, giving faith in both the estimation methods and theoretical procedures. Overall we consider the study to provide an experimental verification of the two estimation procedures using a specific nonlinear multi-DOF WEC.

REFERENCES

[1] J. Hals, J. Falnes, and T. Moan. Constrained optimal control of a heaving buoy wave-energy converter. *Journal of Offshore Mechanics and Arctic Engineering*, 133(1):011401–011401, 2010.

[2] J.A.M. Cretel, G. Lightbody, G.P. Thomas, and A.W. Lewis. Maximisation of energy capture by a wave-energy point absorber using model predictive control. In *Proceedings of the 18th IFAC World Congress*, Milan, Italy, 2011.

[3] F. Fusco and J. V. Ringwood. A simple and effective real-time controller for wave energy converters. *IEEE Transactions on Sustainable Energy*, 4(1):21–30, 2013.

[4] Y. Peña-Sanchez, C. Windt, J. Davidson, and J. V. Ringwood. A critical comparison of excitation force estimators for wave-energy devices. *IEEE Transactions on Control Systems Technology*, pages 1–13, 2019.

[5] B.A. Ling and B.A. Batten. Real Time Estimation and Prediction of Wave Excitation Forces on a Heaving Body. Volume 9: Ocean Renewable Energy, 05 2015.

[6] M. Garcia-Abril, F. Paparella, and J.V. Ringwood. Excitation force estimation and forecasting for wave energy applications. *IFAC-PapersOnLine*, 50(1):14692 – 14697, 2017. 20th IFAC World Congress.

[7] O. Abdelkhalik, Shangyan Zou, G. Bacelli, R. D. Robinett, D. G. Wilson, and R. G. Coe. Estimation of excitation force on wave energy converters using pressure measurements for feedback control. In *OCEANS 2016 MTS/IEEE Monterey*, pages 1–6, 2016.

[8] M. Abdelrahman, R. Patton, B. Guo, and J. Lan. Estimation of wave excitation force for wave energy converters. In *2016 3rd Conference on Control and Fault-Tolerant Systems (SysTol)*, pages 654–659, 2016.

[9] Bingyong Guo, Ron J. Patton, Siya Jin, and Jianglin Lan. Numerical and experimental studies of excitation force approximation for wave energy conversion. *Renewable Energy*, 125:877 – 889, 2018.

[10] Y. Peña-Sanchez, M. Garcia-Abril, F. Paparella, and J. V. Ringwood. Estimation and forecasting of excitation force for arrays of wave energy devices. *IEEE Transactions on Sustainable Energy*, 9(4):1672–1680, 2018.

[11] M. Bonfanti, A.J. Hillis, S.A. Sirigu, P. Dafnakis, G. Bracco, G. Mattiazzo, and A.R. Plummer. Real-time estimation of wave excitation forces for non-linear wave energy converter. *Under review with Ocean Energy*.

[12] H-N. Nguyen and P. Tona. Wave excitation force estimation for wave energy converters of the point-absorber type. *IEEE Transactions on Control Systems Technology*, 26(6):2173–2181, Nov 2018.

[13] W. E. Cummins. The Impulse Response Function and Ship Motions. *Schiffstechnik*, 9:101–109, 1962.

[14] A. Babarit and G. Delhommeau. Theoretical and numerical aspects of the open source BEM solver NEMOH. In *Proceedings of the 11th European Wave and Tidal Energy Conference*, Nantes, France, 2015.

[15] Y. Yu, M. Lawson, K. Ruehl, and C. Michelen. Development and demonstration of the wec-sim wave energy converter simulation tool. In *Proceedings of the 2nd Marine Energy Technology Symposium, Seattle, WA*, 2014.

[16] E. Faraggiana, C. Whitlam, John Chapman, A.J. Hillis, J. Roesner, M. Hann, D. Greaves, Y.-H. Yu, K. Ruehl, I. Masters, G. Foster, and G. Stockman. Computational modelling and experimental tank testing of the multi float wavesub under regular wave forcing. *Renewable Energy*, 2020.

[17] N. Sergiienko, B. Cazzolato, P. Hardy, B. Ding, and M. Arjomandi. Internal-model-based velocity tracking control of a submerged three-tether wave energy converter. In *Proceedings of the Twelfth European Wave and Tidal Energy Conference*, Cork, Ireland, 2017.

[18] A.J. Hillis, C. Whitlam, A. Brask, J. Chapman, and A.R. Plummer. Power capture gains for the wavesub submerged wec using active control. In D. Vicinanza, editor, *Proceedings of the Thirteenth European Wave and Tidal Energy Conference*, Naples, Italy, Sep 1–Sep 6 2019. EWTEC.

[19] A.S. Zurkinden, F. Ferri, S. Beatty, J.P. Kofoed, and M.M. Kramer. Non-linear numerical modeling and experimental testing of a point absorber wave energy converter. *Ocean Engineering*, 78:11 – 21, 2014.

[20] C.O. Housseine, C. Monroy, and G. de Hauteclocque. Stochastic linearization of the morison equation applied to an offshore wind turbine. volume Volume 9: Ocean Renewable Energy of *International Conference on Offshore Mechanics and Arctic Engineering*, 05 2015.

[21] Rajdip Nayek, Souvik Chakraborty, and Sriram Narasimhan. A gaussian process latent force model for joint input-state estimation in linear structural systems. *Mechanical Systems and Signal Processing*, 128:497 – 530, 2019.